Chapter – 4

Development of Texture in IF Steel by ECAP

4.1 Macrotexture Development in IF Steel Deformed by ECAP

Figure 4.1 (a) displays the variation of orientation distribution function with equivalent strain. Maximum ODF intensity increases rapidly upto ε_{vm}=9, thereafter the increase is marginal. Variation of texture index with equivalent strain is shown in Figure 4.1(b). Texture index also increases rapidly for initial stage of deformation (through ε_{vm}=1.8 to 9) with a steady rise from through ε_{vm}=9 to 24. In Figure 4.1 data points are connected to show the trend.

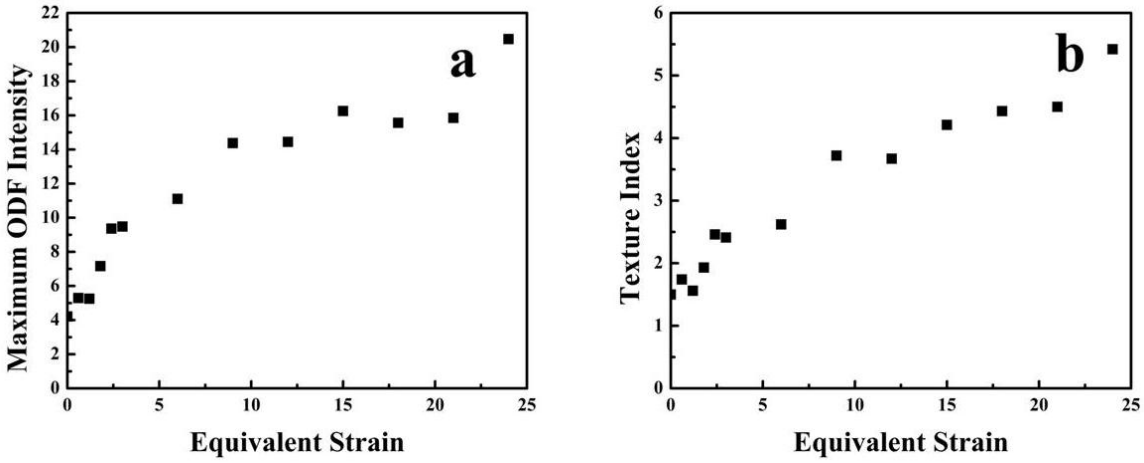

Figure 4.1 Variation of (a) orientation distribution function and (b) texture index with equivalent strain.

Figure 2.6 (a1) gives the color codes for [001] inverse pole figure map, Figure 2.6 (a2) and Figure 2.6 (a3) display reference directions of as-received (or rolled sample) and ECAPed sample on Y-plane respectively. Figure 4.2 gives inverse pole figure maps of as-received and extruded samples respectively. As-received material contains equiaxed grain structures (Figure 4.2(a)) and majority of the boundaries are high angle boundaries (Table

3.1). Figures 4.2(b)-(k) show the inverse pole figure maps of IF steel after various strains. At ε_{vm}=0.6, banded structure forms with high defect density (Figure 4.2(b)). At ε_{vm}=1.2, band thickness decreases. Cells have formed inside the bands at ε_{vm}=1.8 (Figure 4.2(c)). At ε_{vm}=2.4, bands get aligned to deformation direction and cells are formed in the deformation bands (Fig 4.2(e)). Inset displays the cells structure in the material. At ε_{vm}=3, band thickness further reduces along with decrease in their length (Figure 4.2(f)) and their misorientation angle increases giving rise to high angle grain boundary (HAGB) fraction (Table 3.1).

Bands are also aligned to deformation direction. At ε_{vm}=6, HAGBs, deformation bands and cell block boundaries get aligned along deformation direction and form lamellar structures (Figure 4.2(g)). The inset produces the details of lamellar structure. At ε_{vm}=9, the inter lamellar spacing gets reduced and it becomes one to two subgrain wide. Such band of one or two subgrain width is called ribbon grain. The magnified view of the ribbon grains are shown in the inset (Figure 4.2(h)). At ε_{vm}=15, ribbon grains get fragmented into nearly equiaxed grain structures of high angle misorientation containing subgrains. The near-equiaxed grain structure is shown in the inset (Figure 4.2(i)). This fragmentation continues till ε_{vm}=18 and grain size decreases continuously. However, ribbon grains exist at this stage. Through ε_{vm}=21 to 24, nearly equiaxed grain structure is formed (Figure 4.2(j)-(k)) and HAGB fraction as well as grain size saturates (Table 3.1).

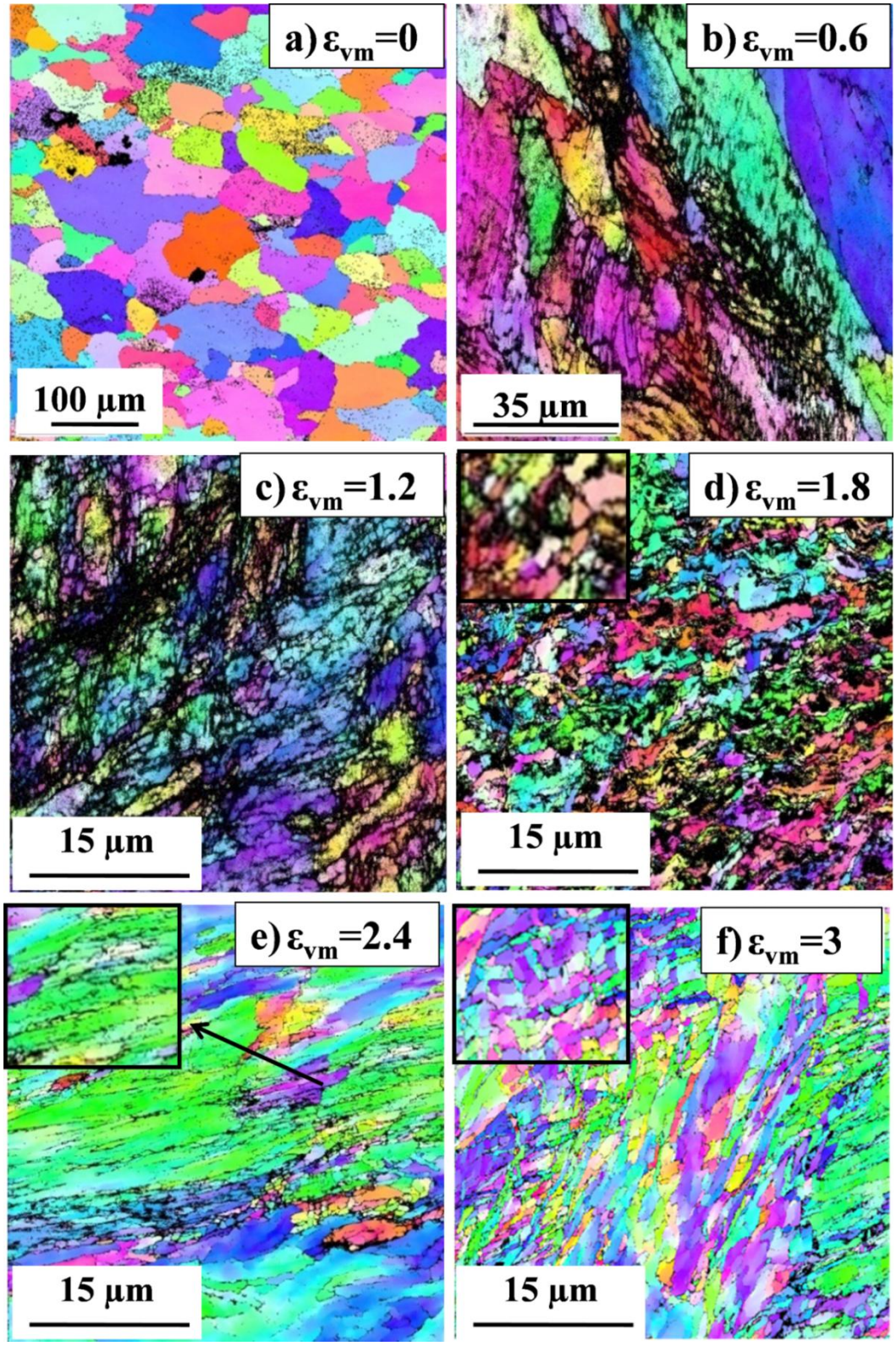

Figure 4.2: [001] Inverse pole figure maps of IF steel after ECAP for (a) as-received, ε_{vm}=0 and after ECAP for (b) ε_{vm}=0.6, (c) ε_{vm}=1.2, (d) ε_{vm}=1.8, (e) ε_{vm}=2.4 and (f) ε_{vm}=3.

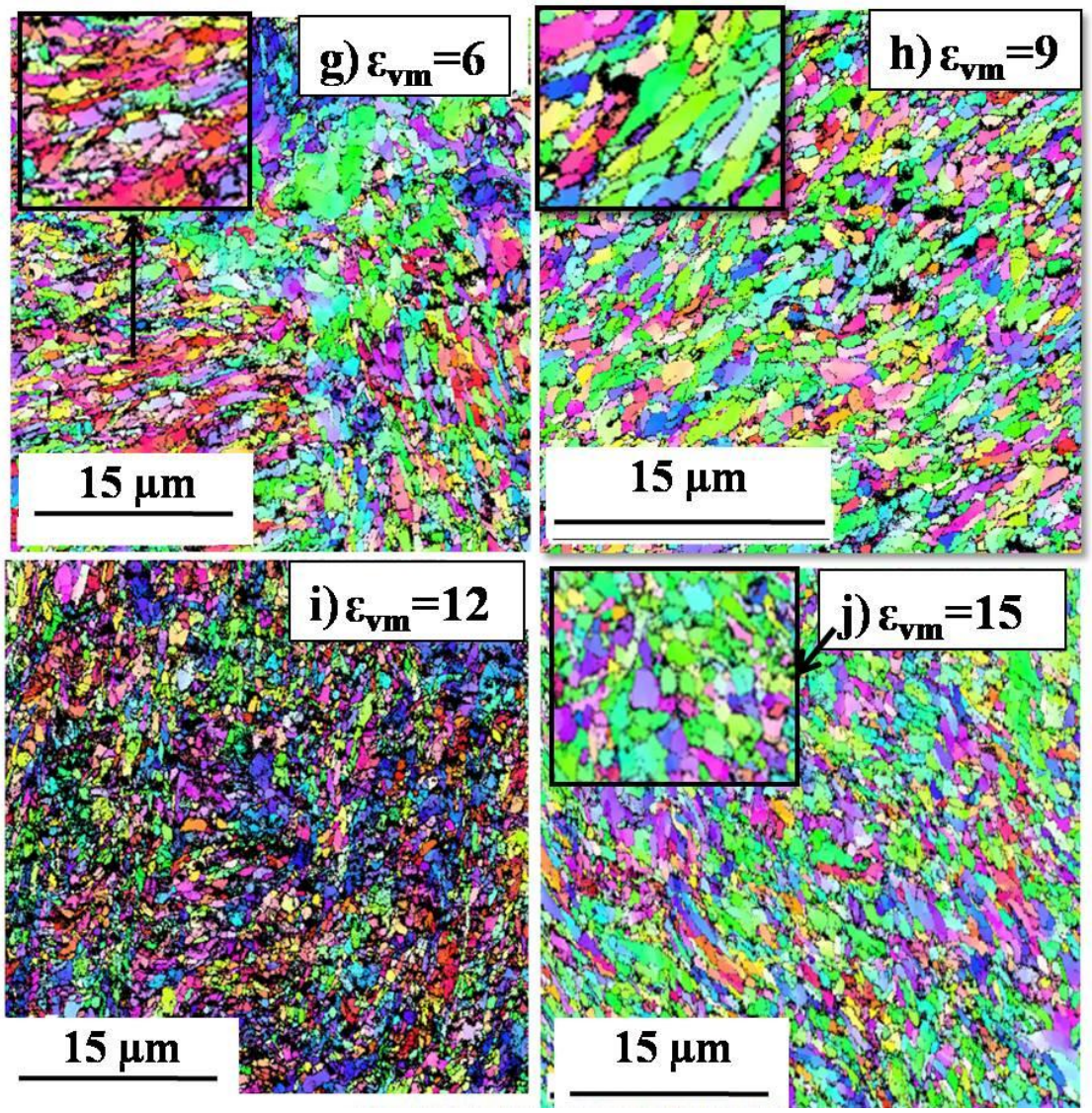

Figure 4.2: [001] Inverse pole figure maps of IF steel after ECAP for (g) ε_{vm}=6, (h) ε_{vm}=9, (i) ε_{vm}=15, (j) ε_{vm}=21.

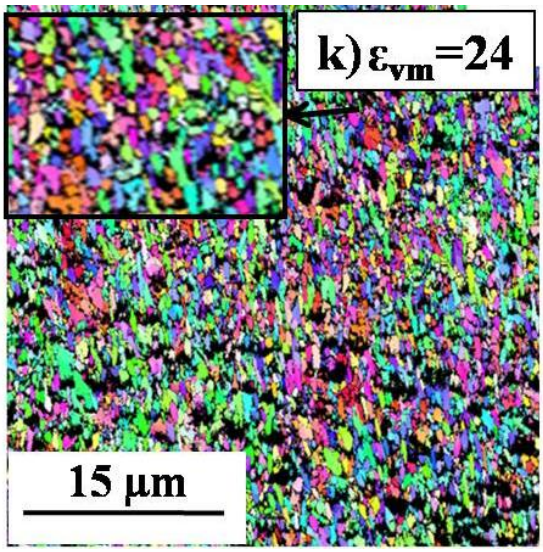

Figure 4.2: [001] Inverse pole figure map of IF steel after ECAP for (k) ε_{vm}=24.

Figures 4.3 (a1)-(k) show the (110) pole figure of IF steel for ε_{vm}=0 to 24. As-received material (ε_{vm}=0) has almost random texture (Figure 4.3(a1)), reference frame of directions are shown in the Figure 4.3a1(or Fig 2.3b). Directions for pole figures of ECAPed material are shown in Figure 4.3a (or Figure 2.3a). At the initial stage of deformation (ε_{vm}=0.6-6), pole figures show that there is no clear fiber texture instead individual components become gradually strong with increasing equivalent strain. Ideal orientations in simple shear in BCC materials are summarized by Beyerlein et al.[Beyerlain et al.2005, Table 1.1]. In the present investigation, at ε_{vm}=0.6, both {110} and <111> fiber components, J_θ , $\bar{J}_\theta$, E_θ , $\overline{E_\theta}$ are formed with weak intensity (Figure 4.3(a)). Reference frame of sample directions are shown in Figure 4.3(a) and 2.3(a,b). These frames will be applied for all other ECAPed samples. At ε_{vm}=1.2, distribution of textures is totally changed, no fiber texture is discernable (Figure 4.3(b)). At ε_{vm}=1.8 weak $D_{2\Theta}$ is formed and E_θ / $\overline{E_\theta}$ components look stronger compared to previous deformation stage (Figure 4.3(c)).

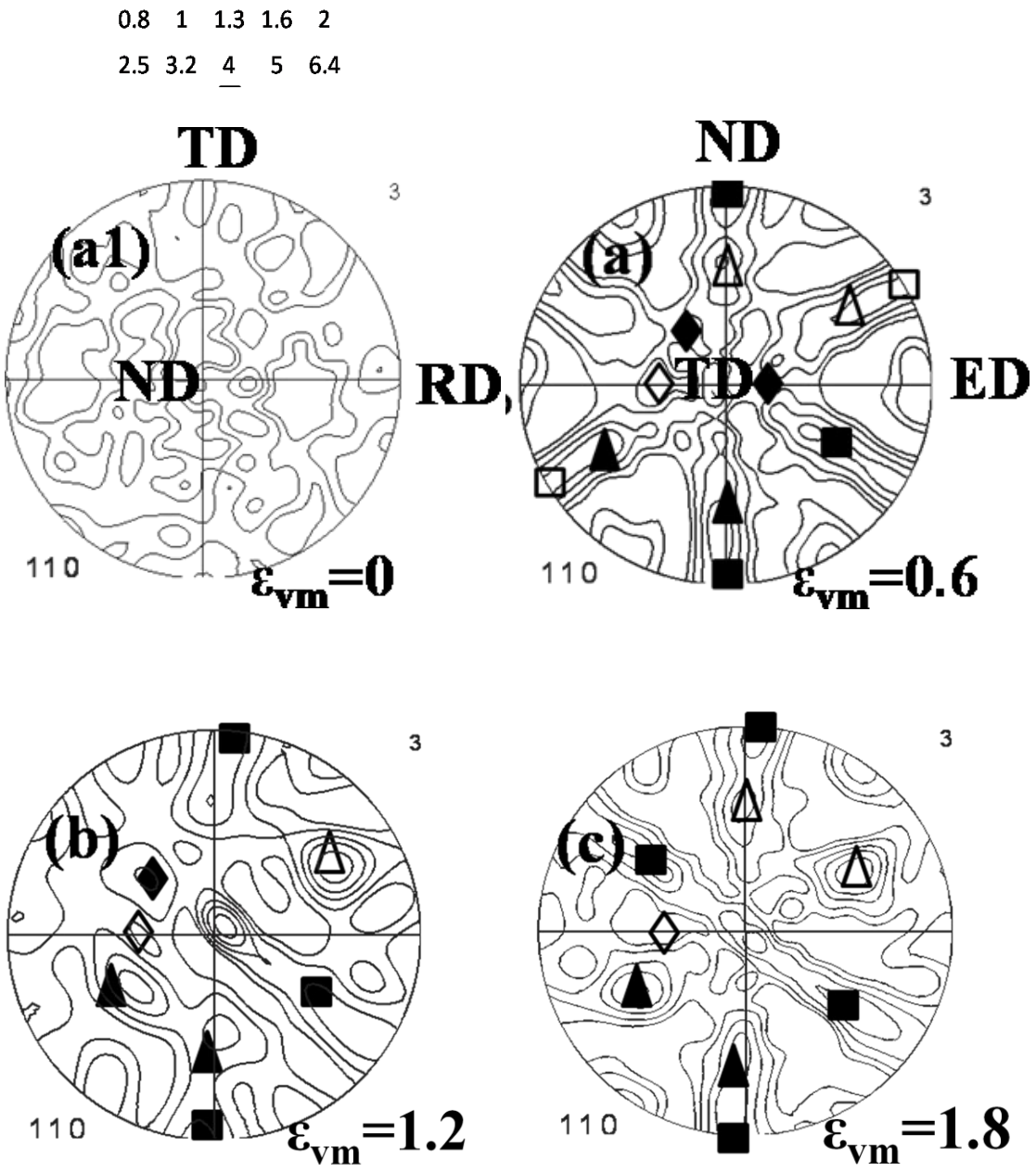

Figure 4.3: (110) pole figure maps of IF steel for (a1) ε_{vm} =0 and after ECAP for (a) ε_{vm} =0.6.
(b) ε_{vm} =1.2 and (c) ε_{vm} =1.8.

The $E_\theta / \overline{E_\theta}$ and $D_{2\Theta}$ components continue to be more concentrated with increasing strain (ε_{vm}=2.4-9) (Figure 4.3(d)-(g)).

At ε_{vm}=9, <111> fiber texture begins to develop clearly (Figure 4.3(g)). Components are rotated about its mean position by ~11° around transverse direction.

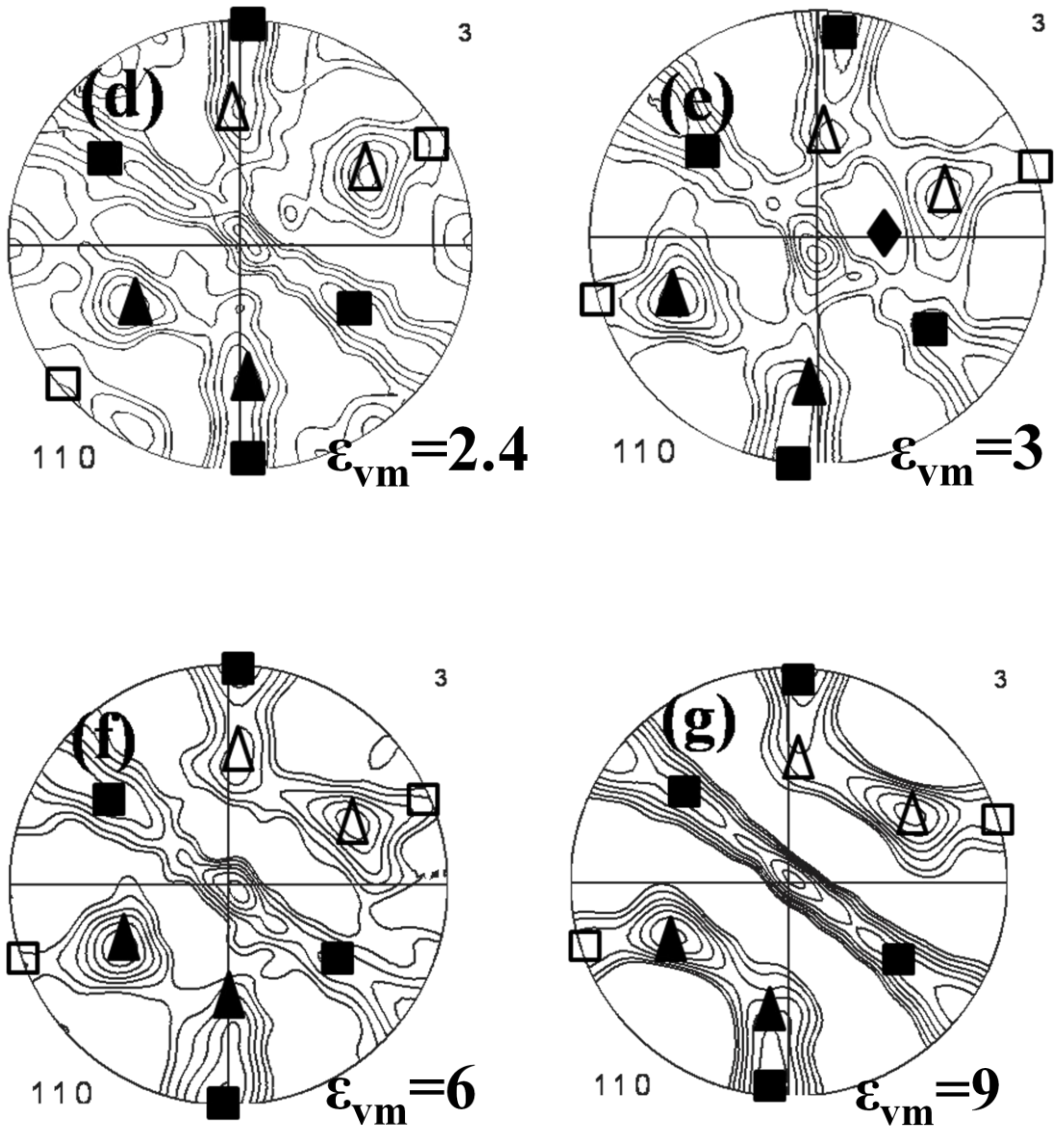

Figure 4.3: (110) pole figure maps of IF steel for (d) ε_{vm} =2.4, (e) ε_{vm} =3, (f) ε_{vm} =6 and (g) ε_{vm}=9.

Through ε_{vm}=15 to18, $D_{1\Theta}/D_{2\Theta}$ and $E_\theta / \overline{E_\theta}$ components continue to increase in intensity and become concentrated (Figure 4.3(h)-(i)). E_Θ and $\overline{E_\theta}$ move towards $D_{1\Theta}$ and $D_{2\Theta}$ upto ε_{vm}=18(Figure 4.3(i)). At ε_{vm}=21, $D_{1\Theta}$ is suppressed but $D_{2\Theta}$ component is

present and E_θ / $\overline{E_\theta}$ get concentrated at their exact position (Figure 4.3(j)). Fully developed <111> fiber is observed through ε_{vm}=15 to 24(Figure 4.3(h)-(k)). Monoclinic symmetry is developed around transverse direction (Figure 4.3(h)-(k)).

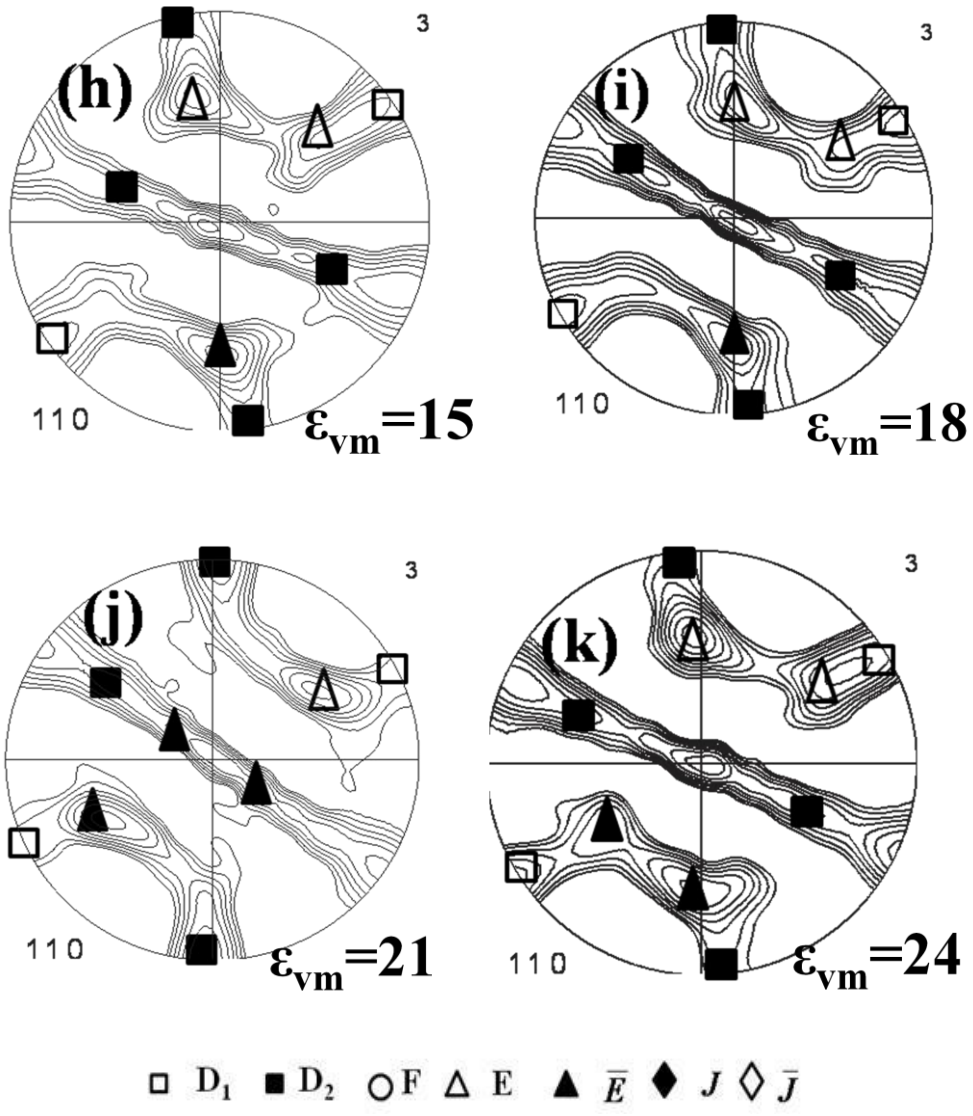

Figure 4.3: (110) pole figure maps of IF steel for (h) ε_m =15 (i) ε_{vm} =18, (j) ε_{vm} =21 and (k) ε_{vm}=24.

Pole figures give idea of fiber texture but it is difficult to predict ideal orientation position because many orientations overlap therefore orientation distribution function (ODF) is calculated to predict an idea of exact orientation. Here Φ_2=0° and 45° sections

of ODFs are given in figure 4.4 (1,2). Random texture is displayed in the entire ODF space (or Euler space) of as-received IF steel not only the Φ_2= 0°or 45° section even though we have shown only this section (Figure 4.4(a2)) as representative. As deformation starts (ε_{vm}=0.6), evolution of new $J_\theta, \bar{J}_\theta$ components of low intensity take place (Figure 4.4b1,b2). At ε_{vm}=1.2, distribution of the orientations changes where intensities of $J_\theta, \bar{J}_\theta$ are reduced (Figure 4.4(c1,c2)). At ε_{vm}=1.8, strong $J_\theta, \bar{J}_\theta$ components are present and are shifted towards $E_\theta, \bar{E}_\theta$.

Texture index (TI) also attains increasing trend (TI=1.9) (Figure 4.4(d2)). Both $\bar{J}_\theta$ and J_θ form concentrated cloud of high intensity at ε_{vm}=2.4 in 45° section (Figure 4.4(e1,e2)). At ε_{vm}=3, $D_{2\Theta}$ component of low intensity has evolved and $\bar{J}_\theta, J_\theta$ have got suppresed. These components are shifted in φ_1 direction (Figure 4.4(f2)). ε_{vm}=6 is the stage where $D_{1\Theta}$, $D_{2\Theta}$ are increased in intensity by suppressing J_θ or $\bar{J}_\theta$ components (Figure 4.4(g1, g2)). Texture index begins to increase at slow rate (TI=2.6) (Figure 4.1a). At ε_{vm}=9, $D_{1\Theta}$, $D_{2\Theta}$ and F give high intensity and concentrated contours shift in negative φ_1 direction in both Φ_2=0° and Φ_2=45° sections (Figures. 4.4(h1, h2)).

The intensity of $D_{2\Theta}$ is less than $D_{1\Theta}$. TI also increases rapidly to 3.7 (Figure 4.1). Further deformation (ε_{vm}=15-18) leads to increase in intensity of $D_{1\Theta}$, $D_{2\Theta}$ (Figures 4.4(i1, i2, j1, j2)). $D_{1\Theta}/D_{2\Theta}$ components continue to shift in -φ_1 direction. $D_{1\Theta}$ is having high intensity compared to $D_{2\Theta}$ but E_θ and $\bar{E}_\theta$ are having low intensity. At ε_{vm}=21 texture index is nearly saturated. $\bar{J}_\theta$ and $\bar{E}_\theta$ components of lower intensity get evolved, $D_{1\Theta}/D_{2\Theta}$ components decrease in intensity. All major components remain at their exact position at ε_{vm}=21 (Figures 4.4(k1, k2)). Material regains TI and its value increases to 5.4 at ε_{vm}=24.

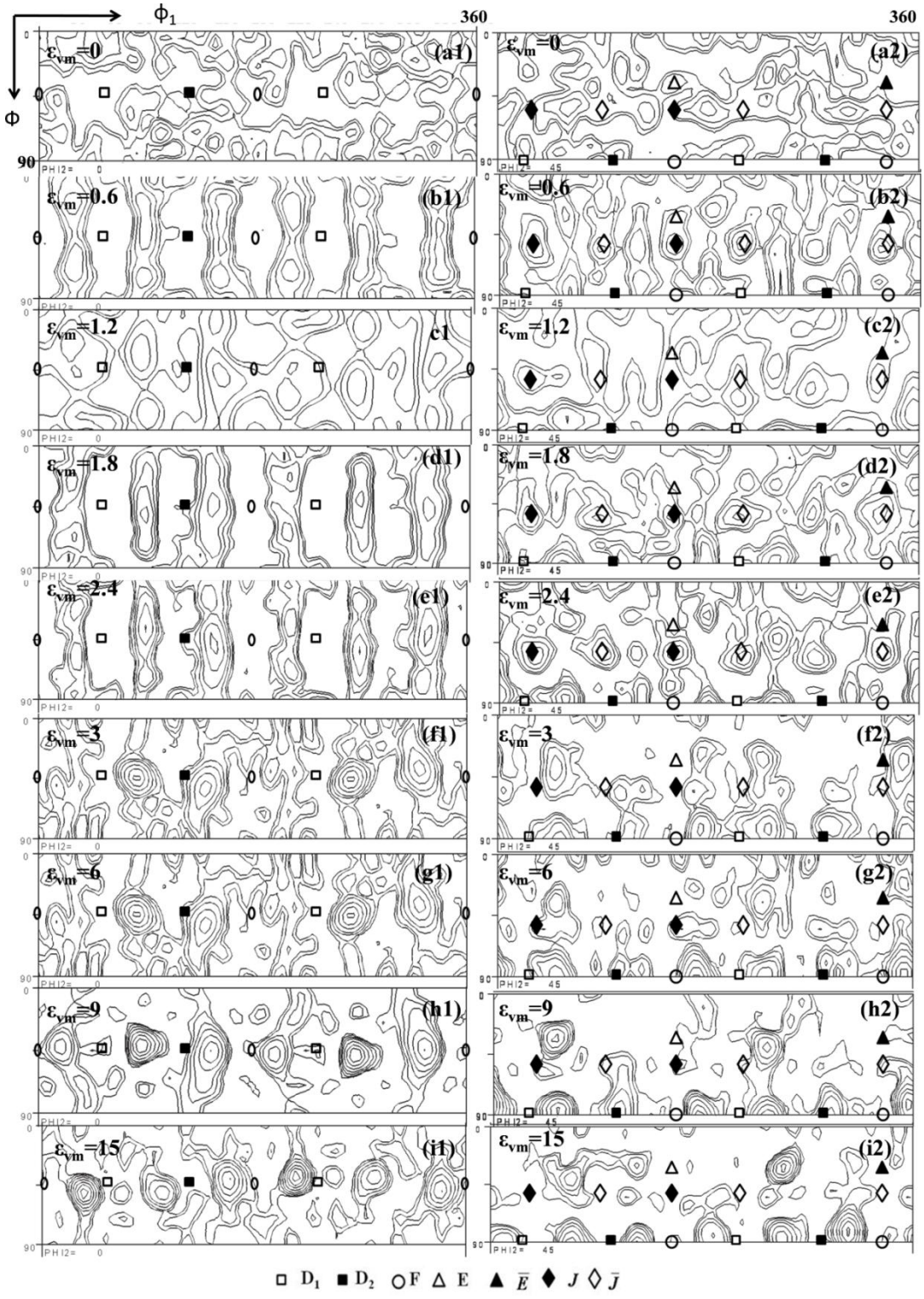

Figure 4.4: ODF maps of IF steel for (a1,a2) ε_{vm}=0 and after ECAP for (b1,b2) ε_{vm}=0.6, (c1,c2) ε_{vm}=1.2, (d1,d2) ε_{vm}=1.8, (e1,e2) ε_{vm}=2.4, (f1,f2) ε_{vm}=3, (g1,g2) ε_{vm}=6, (h1,h2)

ε_{vm}=9 and (i1,i2) ε_{vm}=15, where subscripts 1,2 stand for φ_2=0 and 45° sections respectively.

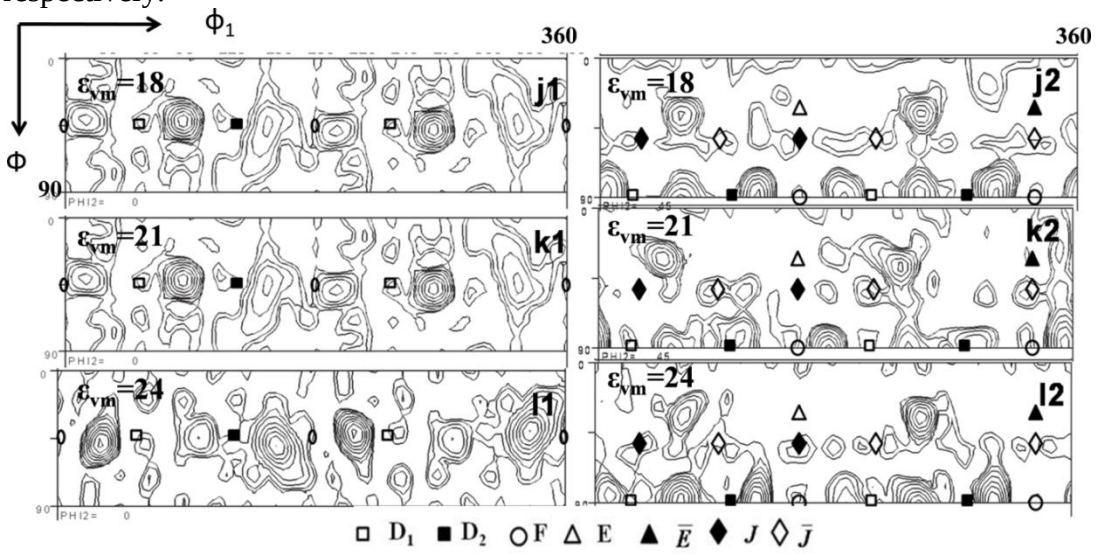

Figure 4.4: ODF maps of IF steel after ECAP for (j1,j2) ε_{vm}=18, (k1,k2) ε_{vm}=21 and (l1,l2) and ε_{vm}=24, where subscripts 1,2 stand for φ_2=0 and 45° sections respectively.

4.2 Microtexture Development in IF Steel Deformed by ECAP

Microtexture provides information about the orientation distribution of individual grains. As-received material shows random texture (Figure 4.5a1). Reference frame for pole figure generated from EBSD data of as-received material is shown in Figure 4.5a1 (or Figure 2.6a2). Weak components of $D_{1\Theta}$, $D_{2\Theta}$, $\bar{J}_{\theta}$ and $E_{\Theta}/\overline{E_{\theta}}$ are observed at ε_{vm}=0.6 (Figure 4.5(a)). Reference frame of directions for pole figures (generated from EBSD data) of ECAPed samples is shown in Figure 4.5a (or 2.6a3). In the localized area (at ε_{vm}=1.2), $\bar{J}_{\theta}$ is weak but $D_{2\Theta}$, $E_{\Theta}/\overline{E_{\theta}}$ are concentrated and strong. Components are shifted from their exact angular position which shows that components are not aligned with macroscopic shear plane and direction (Figure 4.5(b)). At ε_{vm}=1.8, $D_{1\Theta}$ is suppressed, $D_{2\Theta}$, $\bar{J}_{\theta}$ and $E_{\Theta}/\overline{E_{\theta}}$ are present. But E_{Θ} is dominating over $\overline{E_{\theta}}$ (Figure 4.5(c)). At ε_{vm}=2.4, $\overline{E_{\theta}}$ and weak $D_{1\Theta}$ are present (Figure 4.5(d)). $D_{1\Theta}$ component is shifting towards $\bar{E}_{\Theta}$ Weak $E_{\Theta}/\overline{E_{\theta}}$ components are present at ε_{vm}=3 (Figure 4.5(e)), which means

slip is taking place along major slip plane and direction. $E_\Theta/\overline{E_\theta}$ components are moving towards $D_{1\Theta/}$ $D_{2\Theta.}$ Major components which persist at ε_{vm}=6 are $E_\Theta/\overline{E_\theta}$, $D_{1\Theta}/D_{2\Theta}$. $D_{2\Theta}$ is weak compared to $D_{1\Theta.}$ In this case also the components $E_\Theta/\overline{E_\theta}$ are moved toward $D_{1\Theta}$/ $D_{2\Theta}$ (Figure 4.5(f)). Only $E_\Theta/\overline{E_\theta}$ components persist at ε_{vm}=9 (Figure 4.5(g)). $\overline{E_\theta}$ component is stronger than E_Θ. At ε_{vm}=15, {110} and <111> both fibers are visible. Most of the grains are elongated along ND and shear plane normal (SPN). $E_\Theta/\overline{E_\theta}$, $D_{1\Theta}$/ $D_{2\Theta}$ are important components and clear <111> fiber has formed in range ε_{vm}=18-21 (Figures 4.5(i)-(j)). $D_{1\Theta}/D_{2\Theta}$ components are elongated along SPN. $E_\Theta/\overline{E_\theta}$ are shifted towards $D_{1\Theta}/D_{2\Theta.}$ At ε_{vm}=21, all components are at their exact position. $D_{1\Theta}$ component is suppressed at ε_{vm}=24, only $D_{2\Theta}$, $E_\Theta/\overline{E_\theta}$ are persevered.

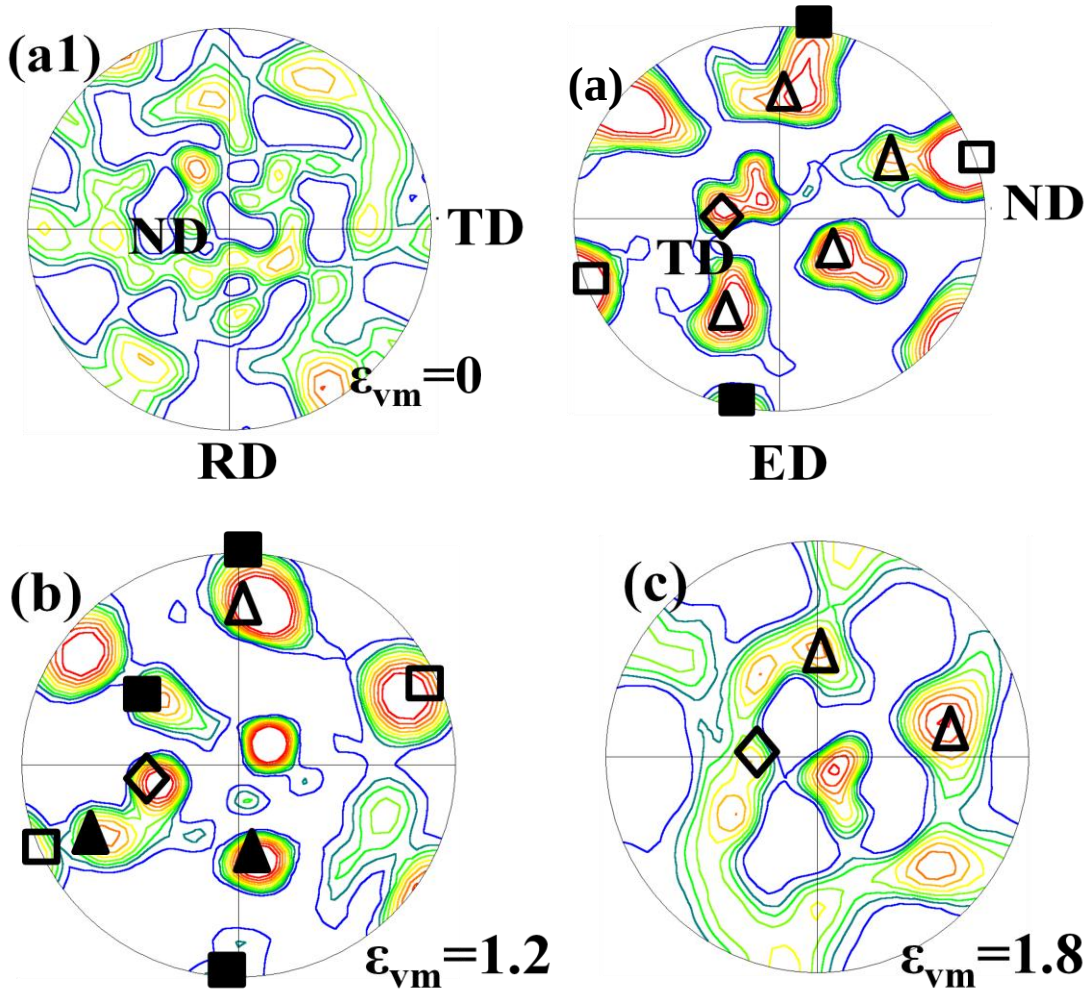

Figure 4.5: (110) pole figure maps of IF steel for (a1) ε_{vm} =0 and after ECAP for (a) ε_{vm} =0.6, (b) ε_{vm} =1.2 and (c) ε_{vm} =1.8.

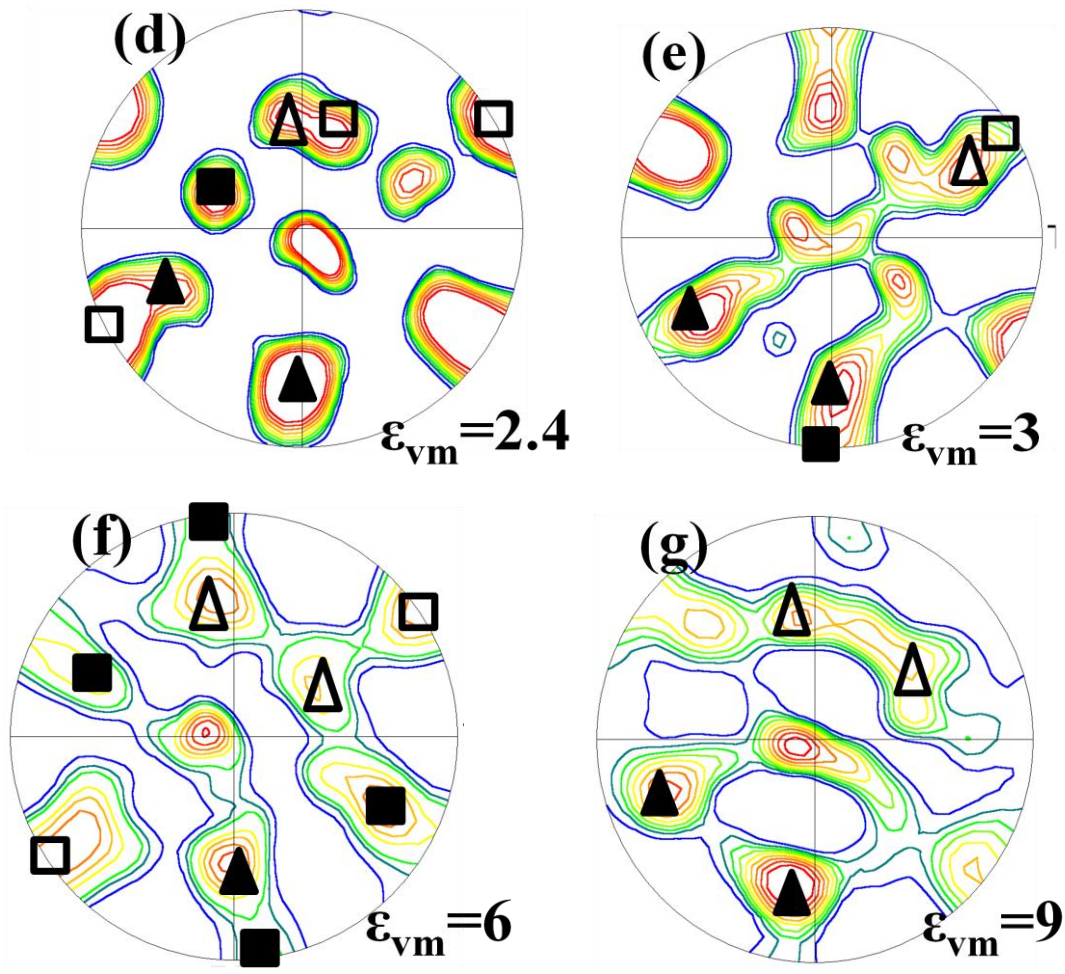

Figure 4.5: (110) pole figure maps of IF steel after ECAP (d) ε_{vm} =2.4, (e) ε_{vm} =3, (f) ε_{vm} =6 and (g) ε_{vm} =9.

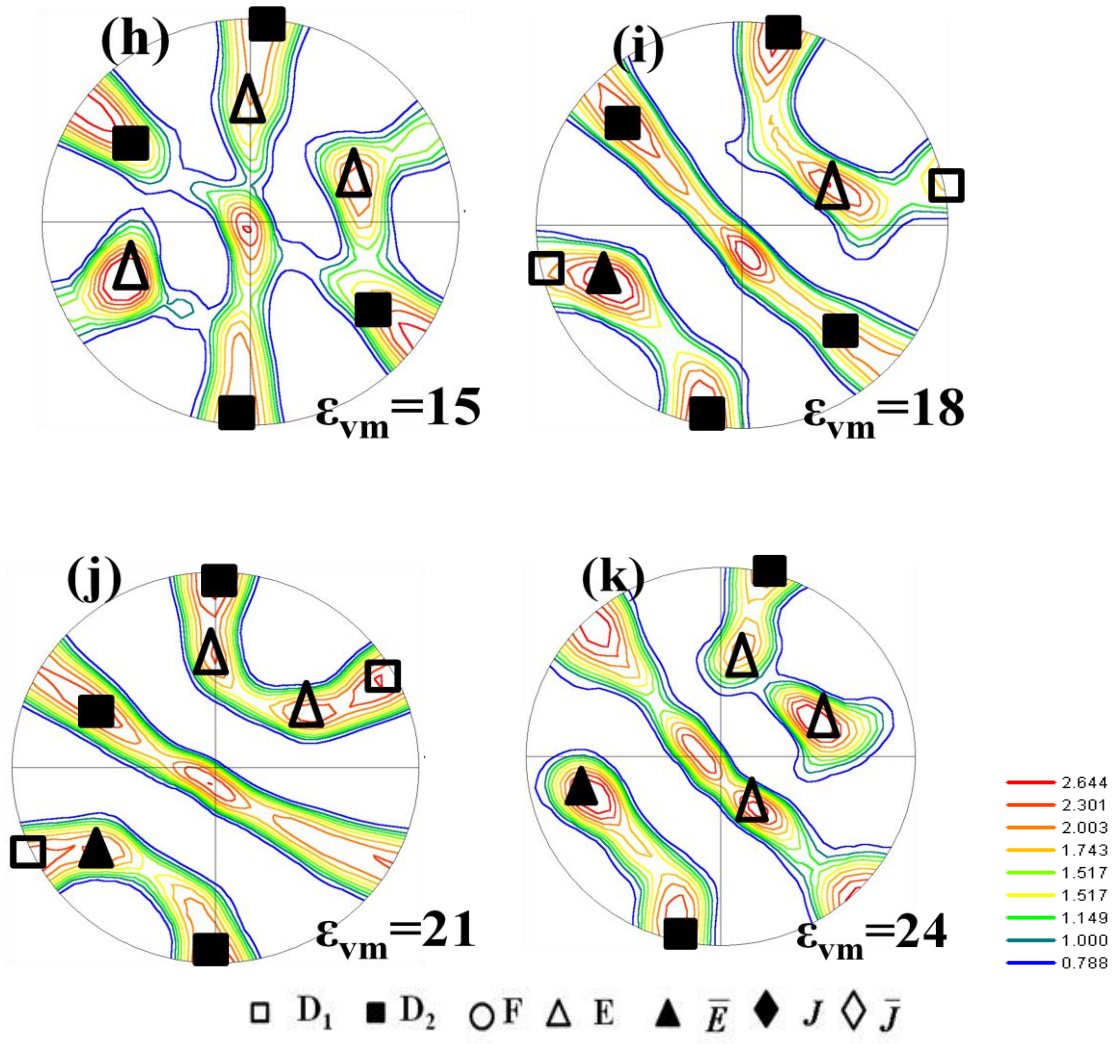

Figure 4.5: (110) pole figure maps of IF steel after ECAP for (h) ε_{vm} =15 (i) ε_{vm} =18, (j) ε_{vm} =21 and (k) ε_{vm} =24.

4.3 Discussion

Effect of Texture on Microstructure Development

Texture is represented by {hkl} <uvw>, which means that orientations of the grains in the billet are such that their {hkl} planes lie parallel to the shear plane, whereas their <uvw> directions lie parallel to the shear direction. The ideal orientations for bcc materials in simple shear are identified in Ref. [Hazra, Gazder, Carman, Pereloma et al. 2011, Messemaeker et al. 2005, Baczynski et al. 1996]. As-received IF steel contains coarse grained equiaxed microstructure (Figure 4.2(a)) containing random texture (Figure

4.3(a1)). In route Bc, sample is rotated 90º always in one direction after each pass which introduces shear on consequent passes. Texture changes gradually but significantly from ε_{vm}=0.6 to 9 with maximum ODF intensity of 3.7. At ε_{vm}=0.6, formation of both {110} and <111> fiber components is a signature of severity of deformation at single pass, alignment of coarse grains in the direction of deformation leads to increase texture intensity to 1.7 at initial stage of deformation. By the severity of applied strain, coarse grains get split into deformation bands due to instability, while neighbouring grains generate inhomogeneous stresses that cause plastic deformation [Humphreys 1995] as well as cell blocks within bands.

At ε_{vm}=1.2, dislocation density increases, thickness of deformation bands decreases and HAGB fraction decreases to lower value. Pole figure (Figure 4.3(b)) and ODF plot (Figure 4.4(c)) show that distribution of orientations is changed at ε_{vm}=1.2 and intensities of texture components developed at lower strain got reduced. The components of pole figure maps at ε_{vm}=1.8 (Figure 4.3(c)) are different from the one generated at ε_{vm}=0.6 (Figure 4.3(a)) as texture of sample entering the die is initially resistant to simple shear texture of subsequent pass. Once flow begins, grains get easily oriented in simple shear direction (after ε_{vm}=2.4) [Beyerlein et al. 2003]. Through ε_{vm}=1.8 to 2.4, cells and cell blocks are formed within bands by rearrangement of dislocations. At ε_{vm}=2.4, cell blocks get aligned to deformation directions. Formation of components of {110} fiber, $\bar{J}_{\theta}$, J_{θ} increases TI value significantly. At ε_{vm}=3, fragmentation of bands are initiated. It is well known that intensity in shear tube increases with equivalent strain as billets are rotated 90º after every pass [Messemaeker et al. 2005]. However, fragmentation of grains lead to slight decrease in TI by suppressing $\bar{J}_{\theta}$, J_{θ} and forming new $D_{2\Theta}$ component of

low intensity. At ε_{vm}=6, high angle grain boundaries, cell blocks and deformation bands get aligned to deformation direction and formation of lamellar grains take place with strong $D_{1\Theta}$, $D_{2\Theta}$ by suppressing all other components. Intensity of $D_{2\Theta}$ is more compared to $D_{1\Theta}$ with maximum ODF intensity of 11.1.

At ε_{vm}=9, inter lamellar spacing gets reduced and becomes single subgrain wide and such single subgrain wide lamellar grains are named ribbon grains (Figure 4.2(h)). The ODF intensity value increases and reaches 14.3 (Figure 4.1(b)) by increasing intensity of $D_{1\Theta}$, $D_{2\Theta}$ and F components that means most of dislocations are gliding along {112} planes parallel to shear plane. At ε_{vm}=15 ribbon grains split into equiaxed grains (Figure 4.2(j)) and fragmentation continues and grains separated from parent grains do not attain random or new orientations but texture index increases marginally. At this strain range only <111> fiber exists which means only those components exist in which <111> direction is aligned with shear plane normal. Grain size also attains a steady trend (Table 3.1). $D_{1\Theta}$, $D_{2\Theta}$ orientations are concentrated cloud instead of random spread in φ and φ_1. Through ε_{vm}=15 to 21, grain refinement attains saturation but material gets textured with increase in intensity of $D_{1\Theta}$, $D_{2\Theta}$ though the rate of increase slows down with increasing strain. Therefore texture intensity increases slightly (Figure 4.3(i)-(j)). Through ε_{vm}=21 to 24, grain size remains almost unchanged and near-equiaxed gains are formed (Figures 4.2(j)-(k)). The same type of trend is observed for ODF intensity (Figure 4.1(a)) which is expected to be correlated to saturation in grain refinement process (Table 3.1). Texture index increases 20 times compared to that of as-received material at ε_{vm}=24 with slight change in intensity of $D_{1\Theta}$ and $D_{2\Theta}$. There is no texture symmetry upto ε_{vm}=6 due to 90º rotation of billet about extrusion direction but monoclinic symmetry is

observed after ε_{vm}=9 (Figure 4.3(g)-(k)). It pertains to the fact that after ε_{vm}=9, texture develops in all consecutive passes leading to alignment of texture components at a symmetric position even though it is not uniform. Generally it was observed in literature that there is no symmetry for route Bc [Pereloma et al. 2005] in ECAP process.

Comparison of Macrotexture with Microtexture

The analysis of present macrotexture and microtexture results suggest that the textures developed in multi-pass ECAP of IF steel can reasonably be characterized by orientations along the {1 1 0} and <111> fibers (Figures 4.3(g)-(k)). Both type of PFs show that $E_\Theta/\overline{E_\theta}$ and $D_{1\Theta}$/ $D_{2\Theta}$ are main orientations for all stages of ECAP process whereas, ODF map shows that $\bar{J}_\theta, J_\theta$ are also important. There is a tendency for orientation flow from $E_\Theta/\overline{E_\theta}$ to $D_{1\Theta}/D_{2\Theta}$ (Figures 4.5(f)-(j)) with increase in strain. Components are not located at their exact positions. In other words components are not aligned along macroscopic shear plane and directions. They are shifted from their ideal position at low equivalent strain level and subsequently come back to its exact position with increase in strain. Deviation from ideal texture positions are summarised for ECAPed materials by Beyerlein and Tóth [Beyerlein et al. 2009]. These deviations can be as high as 20º. The deviations are due to variation in initial texture, applied shear strain, formation of banded structure and subgrains at low strain, change of misorientation angle and shape of grains [Tóth et al. 2004, Li et al. 2005]. The orientation of the two channels of die's intersection plane and the deviation of deformation from simple shear along this plane are the two main factors that together contribute to deviation in measured ECAP textures from simple shear [Li, Beyerlein et al. 2005]. Rounded corner at outer angle of ECAP die generates

inhomogeneity in deformation around shear plane that also leads to deviation of ECAP texture from ideal position [Beyerlein et al. 2005].

4.4 Summary

A strong shear texture occurs as a result of equal-channel angular pressing of hot rolled IF steel by adopting the route Bc. At low strain level, ε_{vm}=0.6, components of {110} fiber, J_θ , $\bar{J}_\theta$ and common components of both {110} and <111> fibers, E_Θ, $\overline{E_\theta}$ are existing but their intensity is low. At intermediate strain range ε_{vm}=1.8-6, J_Θ, $\overline{J_\theta}$ and $D_{1\Theta}$, $D_{2\Theta}$ components are concentrating. At higher strain range, ε_{vm}=9-24, <111> fiber texture forms with high intensity of main components, $D_{1\Theta}$, $D_{2\Theta}$. All components get shifted from their exact position at low strain level and come to their ideal position at large strain level. Monoclinic symmetry is noticed after ε_{vm}=9 by route Bc of ECAP process in IF steel. At ε_{vm}=24, texture index approaches a very high value that 3.6 times that of as-received IF steel.

The change in microstructure with equivalent strain is correlated with texture developments. Texture intensity increases with strain due to formation of different texture components at different strain levels. At ε_{vm}=0.6, coarse grains begin to align in the direction of deformation along with splitting into deformation bands. Alignment of cells and cell blocks (at ε_{vm}=2.4) in deformation bands lead to increase in texture intensity with concentrated clouds of $\bar{J}_\theta$, J_θ components. Fragmentation of bands (at ε_{vm}=3) randomise orientations that suppresses $\bar{J}_\theta$, J_θ components. At ε_{vm}=6, high angle grain boundaries, cell blocks and cell structures get aligned to deformation direction to form lamellar structures with mainly $D_{1\Theta}$, $D_{2\Theta}$ as dominating components. At ε_{vm}=9, oriented ribbon

grains result in strong $D_{1\Theta,}$ $D_{2\Theta}$ components with <111> fiber. At ε_{vm}=15, partial conversion of ribbon grains to near-equiaxed grains produces enhanced intensity of $D_{1\Theta}$ and $D_{2\Theta}$ components. Through ε_{vm}=15 to 21, grain refinement attains saturation with further increase in intensity of $D_{1\Theta}$, $D_{2\Theta}$. At ε_{vm}=24 complete near-equiaxed grain formation takes place, leading to increased intensity of $D_{1\Theta,}$ $D_{2\Theta}$ components.